MOLECULAR AND CELLULAR BIOLOGY, July 2006, p. 5015–5022 Vol. 26, No. 13
0270-7306/06/$08.00+0 doi:10.1128/MCB.02419-05

Autotaxin, a Secreted Lysophospholipase D, Is Essential for Blood Vessel Formation during Development

Laurens A. van Meeteren,[1] Paula Ruurs,[1] Catelijne Stortelers,[1] Peter Bouwman,[2] Marga A. van Rooijen,[3] Jean Philippe Pradère,[4] Trevor R. Pettit,[5] Michael J. O. Wakelam,[5] Jean Sébastien Saulnier-Blache,[4] Christine L. Mummery,[3] Wouter H. Moolenaar,[1]* and Jos Jonkers[2]

Division of Cellular Biochemistry and Center for Biomedical Genetics[1] and Division of Molecular Biology,[2] The Netherlands Cancer Institute, Plesmanlaan 121, 1066 CX Amsterdam, The Netherlands; Hubrecht Laboratory, Netherlands Institute for Developmental Biology, 3584 CT Utrecht, The Netherlands[3]; INSERM U586, Unité de Recherches sur les Obésités, 31432 Toulouse, France[4]; and CRUK Institute for Cancer Studies, Birmingham University, Birmingham B15 2TT, United Kingdom[5]

Received 20 December 2005 /Returned for modification 13 March 2006/Accepted 20 April 2006

Autotaxin (ATX), or nucleotide pyrophosphatase-phosphodiesterase 2, is a secreted lysophospholipase D that promotes cell migration, metastasis, and angiogenesis. ATX generates lysophosphatidic acid (LPA), a lipid mitogen and motility factor that acts on several G protein-coupled receptors. Here we report that ATX-deficient mice die at embryonic day 9.5 (E9.5) with profound vascular defects in yolk sac and embryo resembling the $G\alpha_{13}$ knockout phenotype. Furthermore, at E8.5, ATX-deficient embryos showed allantois malformation, neural tube defects, and asymmetric headfolds. The onset of these abnormalities coincided with increased expression of ATX and LPA receptors in normal embryos. ATX heterozygous mice appear healthy but show half-normal ATX activity and plasma LPA levels. Our results reveal a critical role for ATX in vascular development, indicate that ATX is the major LPA-producing enzyme in vivo, and suggest that the vascular defects in ATX-deficient embryos may be explained by loss of LPA signaling through $G\alpha_{13}$.

Autotaxin (ATX), also known as ectonucleotide pyrophosphatase-phosphodiesterase 2, belongs to the nucleotide pyrophosphatase (NPP) family of ectoenzymes and exoenzymes, originally defined by their ability to hydrolyze nucleotides in vitro (8, 15, 44). Full-length ATX is cleaved along the classical export pathway and secreted as a catalytically active glycoprotein (21, 52). ATX was initially isolated as an autocrine motility factor for melanoma cells (45) and later found to promote metastasis and tumor vascularization in nude mice as well as eliciting an angiogenic response in Matrigel assays (31, 32). Hence, ATX may contribute to tumor progression by providing an invasive and/or angiogenic microenvironment for both malignant and stromal cells, a notion supported by growing evidence that ATX expression is upregulated in various invasive and metastatic cancers (4, 18, 22, 28, 43, 55).

The physiological substrate of ATX had remained elusive until it was discovered that ATX is identical to lysophospholipase D (lysoPLD), a secreted enzyme present in plasma and conditioned media that converts lysophosphatidylcholine (LPC) into bioactive lysophosphatidic acid (LPA) (11, 47, 48). LPA stimulates cell proliferation, migration, and survival by acting on specific G protein-coupled receptors (GPCRs) that are linked to multiple G proteins, including $G_{q/11}$, $G_{i/o}$, and $G_{12/13}$ (20, 30). LPA promotes wound healing in vivo and has been implicated in tumor progression, inflammation, vascular disease, and neural development (5, 23, 28, 42, 51). It has now become clear that LPA production, rather than nucleotide metabolism, accounts for the growth factor-like effects of ATX observed in cell culture. Strikingly, the other NPP family members lack intrinsic lysoPLD activity despite the similarity between their catalytic domain and that of ATX (14), implying that ATX/NPP2 is a unique lysoPLD with no functional redundancy within the NPP family.

In addition to converting LPC into LPA, ATX can also hydrolyze sphingosyl-phosphorycholine (SPC) to yield sphingosine 1-phosphate (S1P) (7), a lipid mediator with signaling properties similar to those of LPA, while acting on distinct GPCRs. The physiological significance of the SPC-to-S1P conversion is doubtful, however, since plasma levels of SPC are >1,000-fold lower than those of LPC (26) and ATX hydrolyzes SPC less efficiently than LPC (7); in fact, S1P production can be accounted for entirely by the action of sphingosine kinases, with no need to invoke a role for ATX/lysoPLD activity, as revealed by the analysis of sphingosine kinase knockout mice (29).

ATX is widely expressed, with highest mRNA levels detected in brain, placenta, ovary, and intestine (12, 25, 46), but its in vivo functions remain unknown. In development, ATX is prominent in the floor plate of the neural tube at midgestation (3). To assess the biological importance of ATX and its relationship to downstream LPA signaling, we disrupted the ATX-encoding gene (*Enpp2*) in mice. We show that ATX deficiency leads to embryonic lethality at midgestation due to impaired vessel formation in the yolk sac and embryo proper, strongly reminiscent of the $G\alpha_{13}$ knockout phenotype (34). Our results suggest a key role for ATX-mediated LPA production and downstream G-protein signaling in vascular development.

* Corresponding author. Mailing address: Division of Cellular Biochemistry, The Netherlands Cancer Institute, Plesmanlaan 121, 1066 CX Amsterdam, The Netherlands. Phone: 31-20-512-1971. Fax: 31-20-512-1989. E-mail: w.moolenaar@nki.nl.

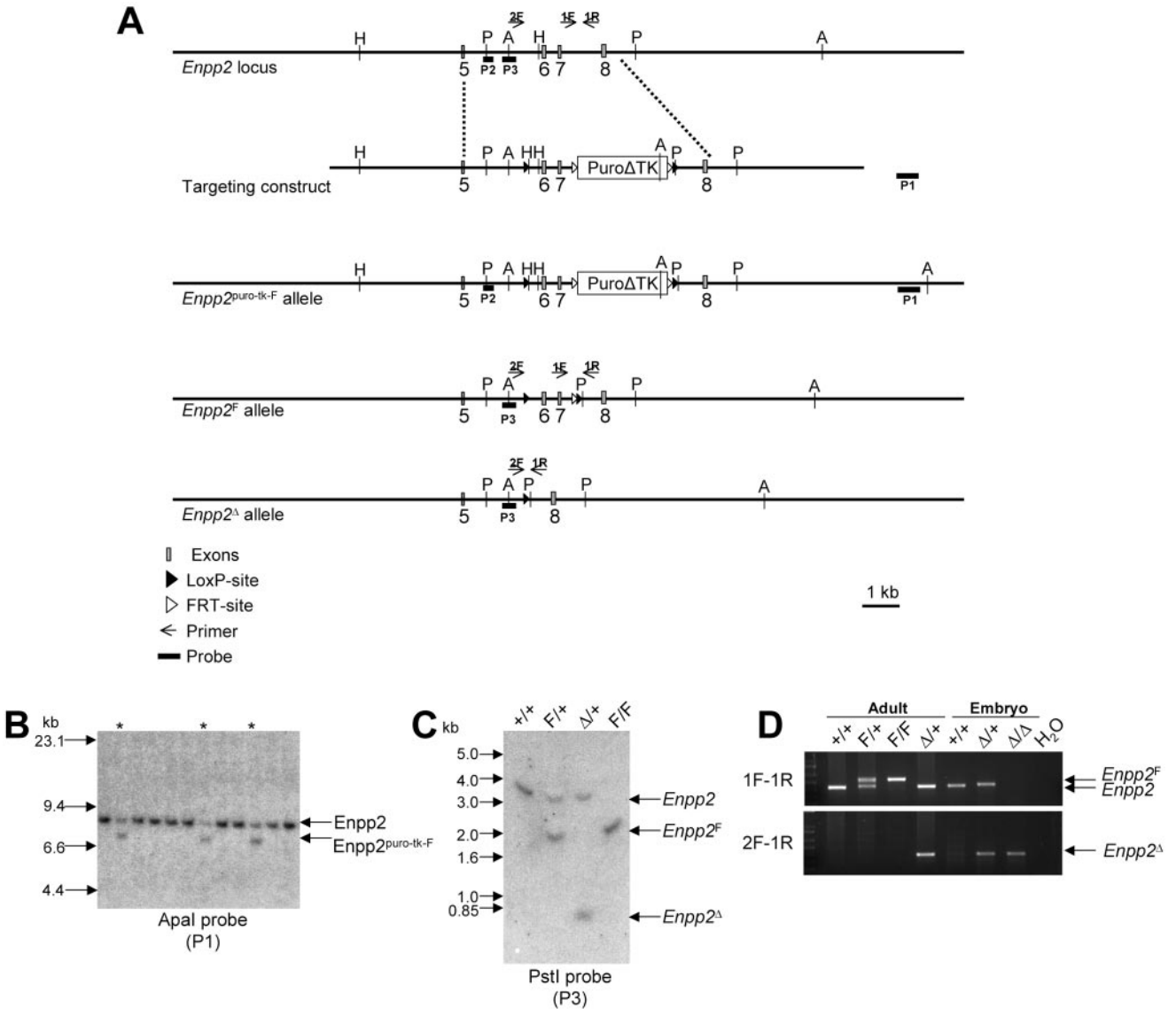

FIG. 1. Generation of conditional *Enpp*$^{F/+}$ mice. (A) Schematic representations of the *Enpp2* locus, the targeting construct, and the mutated *Enpp2* alleles. Exons are indicated by filled boxes, LoxP sites by filled triangles, and FRT sites by open triangles. Probes P1, P2, and P3 are indicated. H, HindIII sites; P, PstI sites; A, ApaI sites. (B) Identification of correctly targeted ES cell clones. Genomic DNA was digested with ApaI and screened with a 3′ flanking probe (P1) located outside the targeting construct. (C and D) Genotyping of adult mice and E9.5 embryos with conditional *Enpp2*^{F} and/or deleted *Enpp2*$^{\Delta}$ alleles by use of PCR with primers 1F, 1R, and 2R or PstI-digested DNA screened with P3.

MATERIALS AND METHODS

Construction of the Enpp2 targeting vector. To generate a conditional *Enpp2*^{F} targeting construct, genomic PAC clones encompassing *Enpp2* were obtained by screening high-density filters of the RPCI-21 mouse PAC library with a cDNA probe containing *Enpp2* exons 6 to 8. Primers with AscI, PvuI, and SbfI restriction sites were designed to amplify a 5.2 kb 5′ flanking fragment, a 1.4 kb central fragment (containing *Enpp2* exons 6 to 7), and a 5 kb 3′ flanking fragment, respectively. PCR amplification was performed with a proofreading DNA polymerase (*Pwo* polymerase; Roche) for 12 cycles to prevent introduction of mutations. After cloning of PCR products in a Zero Blunt TOPO cloning vector (Invitrogen), fragments were excised using the appropriate restriction sites and cloned into the pFlexible targeting vector (49).

Generation of Enpp2$^{F/+}$ ES cells and mice. The targeting construct (Fig. 1A) was linearized with NotI and introduced into 129Ola-derived E14-IB10 embryonic stem (ES) cells by electroporation followed by selection of puromycin-resistant ES clones. Southern blot analysis of ApaI-digested DNA from 192 drug-resistant colonies with a 3′ external probe (probe I) yielded 11 correctly targeted ES clones (Fig. 1B). The presence of the 5′ LoxP site was determined by Southern blot analysis of HindIII-digested ES DNA with the 5′ internal probe P2 (data not shown). Out of seven positive clones, three were used to remove the puroΔTK marker by transient FLP recombinase expression (39). Ganciclovir-resistant colonies were analyzed by PCR using primers 1F and 1R to detect deletion of the puroΔTK cassette and the presence of the 3′ LoxP site. Two independent clones with normal karyotypes were injected into C57BL/6 blastocysts. Chimeric mice born from these embryos were crossed to FVB/N females to produce heterozygous mutant F_1 offspring. All mouse strains used were maintained on a FVB genetic background.

DNA analysis. DNA was isolated from mouse tissues and tail-tip DNA using the Wizard Genomic DNA purification kit (Promega). Southern analysis was performed with 10 μg of genomic DNA digested with the appropriate restriction enzymes. Presence of the LoxP sites and deletion of the floxed exons was determined by Southern analysis of PstI-digested DNA with probe 3 (Fig. 1C).

PCR analysis of genomic DNA was performed with primers 1F and 1R or primers 2F and 1R. Primer set 1F and 1R yields 441 and 540 bp products for the wild-type (wt) and floxed alleles, respectively. Primer set 2F and 1R yields a product of 380 bp for the deleted allele (Fig. 1D). Primer sequences were as follows: for 1F, 5′-CAT TTC CAT TCC CTG CTC C-3′; for 1R, 5′-ACA GAC TTC TCT GAA GCT GAC-3′; and for 2F, 5′-GCA CAT ACC TTT AAT TCC AGC AC-3′.

DNA probes. Probe 1 was a 280-bp fragment of Enpp2 intron 8, produced by PCR amplification with primers 5′-GCATCTGCTGATCTCCGGAG-3′ and 5′-CCAAGCATTGTAAAGGCACA-3′. Probe 2 was a 290-bp fragment of Enpp2 intron 5, produced by PCR amplification with primers 5′-GCATCTGCTGATC TCCGGAG-3′ and 5′-CCAAGCATTGTAAAGGCACA-3′. Probe 3 was a 425-bp fragment of Enpp2 intron 5, produced by PCR amplification with primers 5′-GTGTTTAGATATCTTTATTTTTCC-3′ and 5′-GAATATGTGAGTAAT GTATG-3′.

Quantitative RT-PCR. Embryos dissected free of decidua were snap frozen in liquid nitrogen, and total RNA was extracted. First-strand cDNA was synthesized with Superscript II reverse transcriptase (RT) (Invitrogen) and oligo(dT) primers. Real-time RT-PCR was carried out using 6.25 to 12.5 ng cDNA and 300 nM of each oligonucleotide in 25 μl of 1× SYBR green PCR master mix (Applied Biosystems). PCR conditions were 2 min at 50°C and 10 min at 95°C followed by 50 cycles of 15 s at 95°C and 1 min at 60°C. Product sizes were verified by collecting a melting curve from 55°C to 95°C after final amplification. HPRT (hypoxanthine phosphoribosyltransferase) and glyceraldehyde-3-phosphate dehydrogenase were used for data normalization. Standard curves were produced with serial dilutions of a cDNA mix of embryonic day 9.5 (E9.5) and E10.5 wt embryos. The sequences of the primers used were as follows: for Atx-F, 5′-GACCCTAAAGCCATTATTGCTAA-3′; for Atx-R, 5′-GGGAAGGTGCT GTTTCATGT-3′; for Vegfa-F, 5′-TGTACCTCCACCATGCCAAGT-3′; for Vegfa-R, 5′-TGGAAGATGTCCACCAGGGT-3′; for Hprt-F, 5′-CTG GTGA AAAGGACCTCTCG-3′; and for Hprt-R, 5′-TGAAGTACTCATTATAGTCA AGGGCA-3′. Primer sequences for mouse LPA receptor genes have been described previously (17).

Immunohistochemistry. Vascular endothelial cells were visualized by immunohistochemistry using rabbit anti-CD31 (PECAM-1) monoclonal antibody (PharMingen) as described previously (6).

ATX activity and quantification of plasma LPA and S1P levels. Blood was collected and allowed to clot at 37°C for 1 h. Serum was collected by centrifugation at 1,100 × *g* (10 min) followed by centrifugation at 10,000 × *g* (2 min). Serum was incubated overnight at 37°C with 2 μM CPF4, and the decrease in the fluorescent resonance energy transfer (FRET) ratio was measured as described previously (52). LPA was butanol extracted from heparin-treated mouse plasma and quantified using a radioenzymatic assay (38). S1P levels were determined by liquid chromatography-mass spectrometry as described previously (4).

RESULTS

Generation of conditional ATX knockout mice. ATX is encoded by the *Enpp2* gene. We used the Cre-loxP system to generate $Enpp2^{F/+}$ mice carrying a conditional *Enpp2* null allele in which exons 6 and 7, encoding the active center of ATX, are flanked by *loxP* sites (Fig. 1). Intercrossing of heterozygous $Enpp2^{F/+}$ mice produced homozygous $Enpp2^{F/F}$ animals that were phenotypically normal, indicating that insertion of the *loxP* sites did not disrupt essential functions of ATX. To induce germ line inactivation of ATX, $Enpp2^{F/F}$ mice were mated to mice carrying a Cre transgene driven by the β-actin promoter. Cre-mediated deletion of *Enpp2* exons 6 and 7 introduces an early stop codon and removes most of the ATX protein sequence.

ATX-deficient mice die at midgestation with severe vascular defects. Heterozygous $Enpp2^{+/-}$ knockout mice were healthy and fertile. However, no homozygous $Enpp2^{-/-}$ offspring was found among 118 newborn mice from heterozygous intercrosses (Table 1), suggesting that ATX deficiency is lethal at the embryonic stage. To investigate this, embryos were genotyped at different development stages. At E9.5, ATX-deficient embryos could be recovered at the expected Mendelian frequency (Table 1), but all of them showed severe vascular defects in the yolk sac and were retarded in their development. By E10.5, most ATX-deficient embryos were resorbed.

TABLE 1. Genotypes of progeny from ATX heterozygous intercrosses

Stage	% Genotype[a]			Total no. of progeny
	+/+	+/−	−/−	
E7.5	27	45	27	11
E8.5	20	50	30[b]	50
E9.5	27	48	25[b]	103
E10.5	25	60	15[c]	20
P0	32	68	0	118

[a] Genotypes were determined as described in Materials and Methods and Fig. 1 legend.
[b] Embryos were morphologically abnormal, as detailed in Table 2.
[c] All embryos appeared to be necrotic and were partially resorbed.

Strikingly, blood vessels in the yolk sac of ATX-deficient embryos were poorly developed compared to their wt and heterozygous littermates at E9.5. Between E8.5 and E9.5, extraembryonic endothelial cells normally remodel into a vascular network that connects with the embryo proper; the yolk sac then functions as the primary source of nutrients. At E9.5, blood appeared dispersed in the ATX-deficient yolk sac rather than in a vascular network as in wt and ATX heterozygous yolk sacs (Fig. 2A). Mutant yolk sacs showed patched cavities surrounded by endothelial cells and filled with blood cells, while the mesothelial cells on the inner aspect of the yolk sac were rounded rather than flattened (Fig. 2B).

Vessels of ATX-deficient embryos within the nonvascularized yolk sac were strikingly enlarged, particularly in the head region, compared to those of wt and heterozygote embryos at E9.5; however, mutant embryos were not hemorrhagic (Fig. 2C, D, and E and data not shown). To determine whether endothelial cells had differentiated from early angioblasts, we used an antibody to CD31/PECAM, a marker for mature endothelial cells. CD31-positive cells were readily detected in both yolk sac and embryo proper, indicating that ATX deficiency did not impair the differentiation of progenitor cells into endothelial cells (Fig. 2D). Cardiac development appeared to be normal, as judged from heart beating, but was not examined in detail. We conclude that ATX-deficient mice die around E9.5, with circulatory failure being the most likely primary cause of death.

Additional abnormalities in ATX-deficient embryos. A number of additional abnormalities were observed in ATX-deficient embryos at E8.5 and E9.5, as summarized in Table 2. At E9.5, the large majority (85%) of mutant embryos had not initiated axial turning (Fig. 2E), which could reflect generally retarded development. In about 40% of the ATX-deficient embryos analyzed, at E8.5 there was abnormal development of the allantois, which appeared swollen and failed to fuse to the chorion (Fig. 2F). Furthermore, in >80% of the E8.5 mutant embryos, the neural headfold (i.e., the future forebrain) was asymmetric due to enlargement of one of the folds, which showed extremely large cavities or effusions (Fig. 3A and B). Further down the neural axis, we observed large effusions on the dorsal side (Fig. 2E), which displayed massive apoptosis as detected by terminal deoxynucleotidyltransferase-mediated dUTP-biotin nick end labeling assays (data not shown). Such

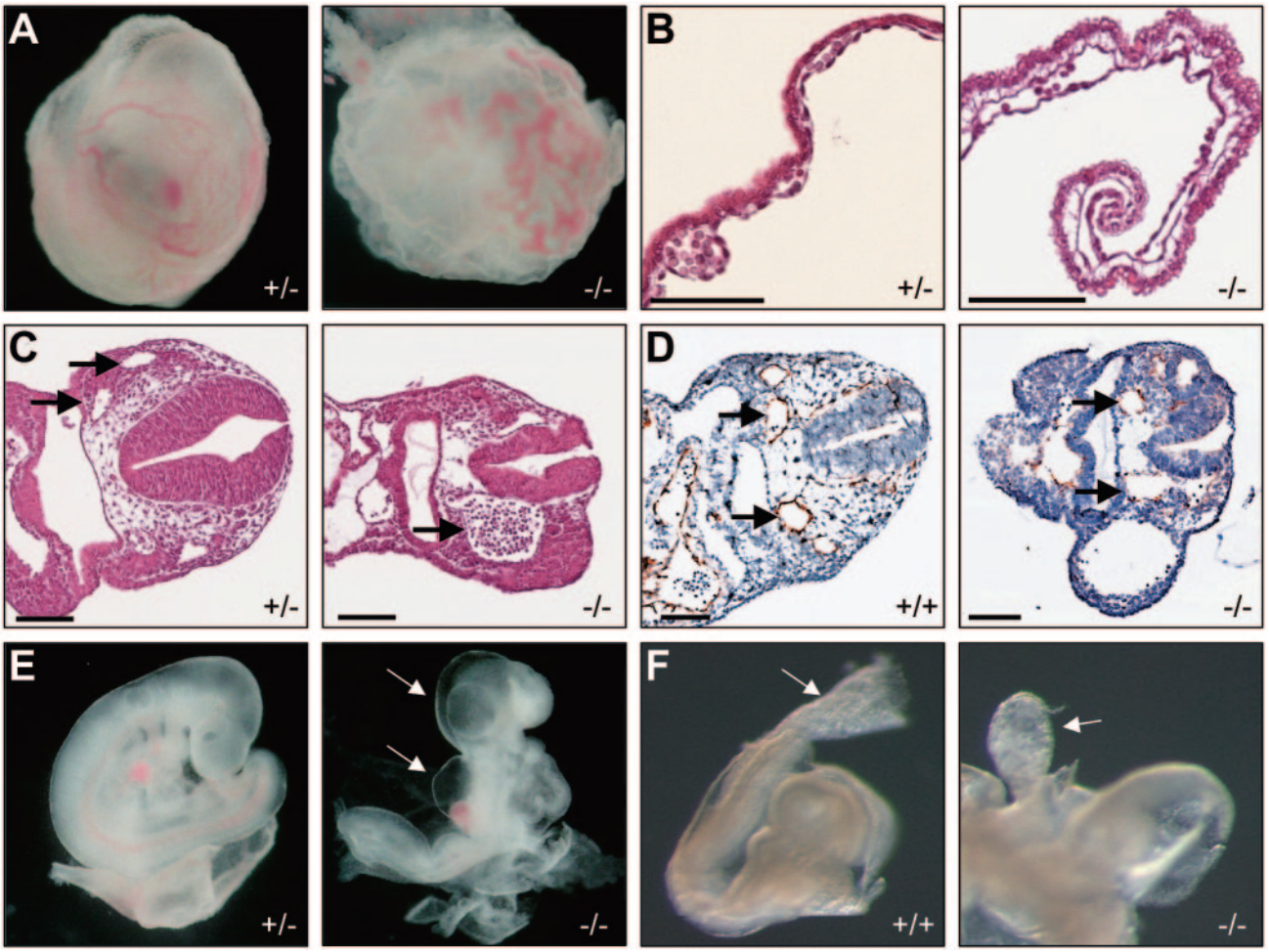

FIG. 2. Phenotype of ATX-deficient yolk sacs and embryos. (A) Yolk sacs of heterozygote (+/−) and ATX-deficient (−/−) embryos at E9.5. Note absence of a visible vascular network in −/− yolk sacs, whereas blood islands are readily detectable. (B) Sections of yolk sacs (hematoxylin and eosin [HE] stained) at E9.5, showing primitive vascular structures containing hematopoietic cells. In mutant yolk sacs, the mesothelial cells on the inner aspect of the yolk sac are rounded rather than flattened. (C) Transverse sections of HE-stained heterozygous or ATX-deficient embryos at E9.5. Note enlarged vessels (arrows) and neural tube malformation in the ATX-deficient embryo compared to the heterozygous control. (D) Transverse sections of HE- and CD31-stained heterozygous or ATX-deficient embryos at E9.5. Note enlargement of CD31-positive vessels in ATX-deficient embryos. (E) Malformation of ATX-deficient embryos at E9.5. Note large effusions in the head region and on the dorsal side (arrows) and no axial turning of the mutant embryo. (F) Malformation of the allantois at E8.5. The allantois (white arrow) appeared short and swollen and failed to fuse to the chorion in mutant embryos. (Scale bars, 100 μm).

effusions are indicative of osmotic imbalance as a consequence of disrupted circulation.

ATX deficiency also led to malformation of the neural tube in the majority of the mutant embryos analyzed: the neural tube had not closed properly at E9.5 and, furthermore, appeared kinked and undulated over its entire length at E8.5, as opposed to the straight neural tube observed in wt embryos (Fig. 2C and D and Fig. 3C and D). Given the prominence of ATX in the floor plate of the neural tube (3), these defects are most likely due to local ATX deficiency and not secondary to circulatory failure or growth retardation. A kinked neural tube is also observed in fibronectin-deficient embryos at this stage (13), suggesting that the neural tube defect associated with ATX deficiency could be due to insufficient extracellular matrix support.

Expression of ATX and LPA receptors during vascular development. We next used quantitative RT-PCR to examine the

TABLE 2. Phenotypic abnormalities in ATX-deficient embryos and yolk sacs[a]

Stage and phenotype	% Penetrance	No. of embryos analyzed
E8.5		
Allantois malformation	41	29
Neural tube malformation	75	12
Dorsal effusions	44	27
Asymmetric headfolds	83	35
E9.5		
No yolk sac vascularization	100	26
Enlarged vessels in embryo	100	4
No axial turning	85	26
Dorsal effusions	42	26
Enlarged head region	54	26

[a] See text for further details.

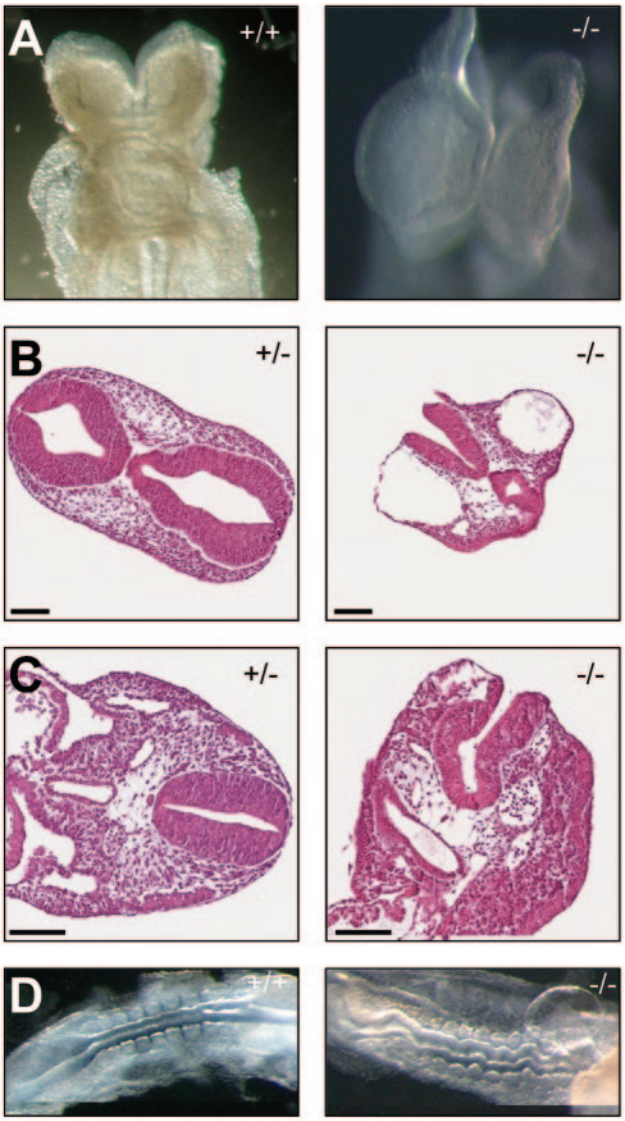

FIG. 3. Headfold asymmetry and neural tube defects in ATX-deficient embryos. (A) Headfold asymmetry in ATX-deficient embryos (E8.5), showing enlargement of one of the headfolds. (B and C) Transverse sections of the head region (E9.5). Note large cavities in the mutant embryos and malformation of the neural tube, which was often unclosed and kinked. (D) Undulated neural tube in ATX-deficient embryos (E8.5), as opposed to the straight neural tube in wt embryos. (Scale bars, 100 μm).

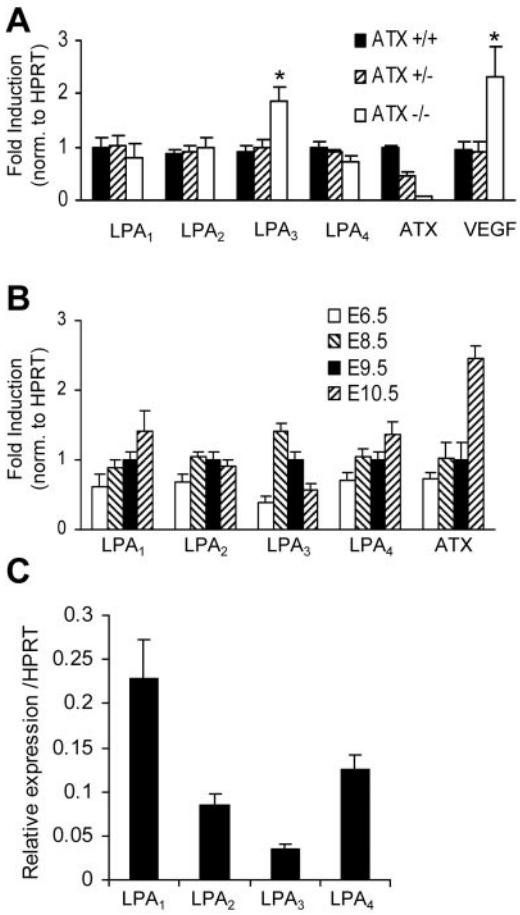

FIG. 4. Expression analysis, as determined by quantitative RT-PCR. (A) Expression patterns of LPA_{1-4}, ATX, and VEGF-A in wt, heterozygous, and knockout embryos at E9.5. Expressions were normalized to HPRT. Note increased VEGF-A expression in the ATX-deficient embryos. (B) Temporal expression pattern of LPA_{1-4} and ATX mRNA levels in developing wt embryos during E6.5 to E10.5. Expression levels were normalized to HPRT. (C) Relative LPA receptor expression patterns in wt E.9.5 embryos.

expression pattern of ATX and the four known LPA receptors (LPA_1 to LPA_4) in wt, heterozygous, and mutant embryos (Fig. 4A). In ATX-deficient and heterozygous embryos, the LPA receptor expression pattern was essentially similar to that in wt embryos (E9.5), although LPA_3 levels were upregulated by approximately twofold in the knockouts (Fig. 4A). Of note, ATX expression in the heterozygotes was 50% of that in the wild types. We also examined the temporal expression pattern of ATX and LPA_{1-4} in wt embryos. ATX and LPA_{1-4} were expressed during early postimplantation stages (E6.5 to E8.5), prior to yolk sac vascular development (Fig. 4B). Expression increased during the stages of vessel formation and expansion (E8.5 to E10.5). ATX, LPA_1, and LPA_4 mRNA levels reached a maximum by E10.5, whereas LPA_3 expression peaked around E8.5 (Fig. 4B). Expression of LPA_1 was significantly higher than that of LPA_{2-4} (Fig. 4C). Expression of ATX in conjunction with all four LPA receptors during E6.5 to E10.5 supports the idea that ATX-regulated LPA production and signaling are important for development during midgestation.

Since vasculogenesis is critically dependent on vascular endothelial growth factor (VEGF) (54) and since LPA induces VEGF-A expression in mouse embryonic fibroblasts (C. Stortelers, unpublished results), we tested whether the vascular phenotype might involve VEGF deficiency. However, VEGF mRNA levels were increased rather than decreased in the ATX-deficient embryos (Fig. 4A). Because VEGF is a hypoxia target gene, the observed increase in VEGF might be due to oxygen deprivation resulting from circulatory failure. Whatever the precise mechanism may be, the results show that increased VEGF production does not rescue the vascular defects resulting from loss of ATX.

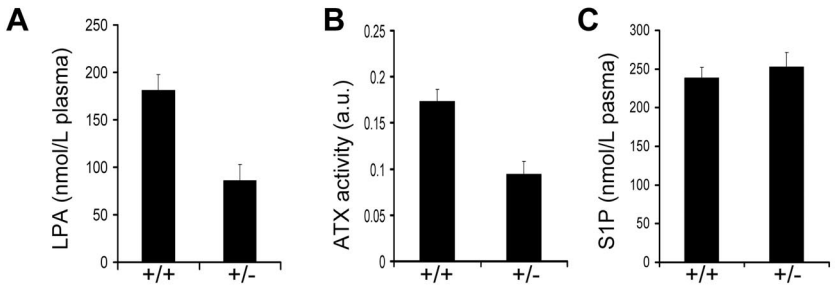

FIG. 5. Determination of plasma ATX activity, LPA, and S1P levels. (A) Half-normal plasma LPA levels in heterozygous ATX mice (86 ± 14 nmol/liter versus 181 ± 17 nmol/liter in the wild types). LPA levels were determined by the generation of phosphatidic acid, produced by the transfer of a ^{14}C fatty acyl chain onto LPA (38). Values correspond to means ± standard errors of the means ($n = 4$). (B) ATX activity in serum as determined by CPF4, the FRET-based ATX sensor (2 μM) (52). Relative ATX activity was calculated as the decrease in the FRET ratio (+/+, $n = 7$; +/−, $n = 5$). a.u., arbitrary units. (C) Normal plasma S1P levels in heterozygous mice, as determined by liquid chromatography-mass spectrometry (heterozygote, $n = 10$; wild type, $n = 13$).

Half-normal ATX activity and plasma LPA levels in heterozygous mice. Since ATX functions as a lysoPLD, ATX deficiency should lead to loss of LPA production. Determination of LPA levels in interstitial fluids from midgestation embryos is technically quite demanding, so we compared serum ATX activity and plasma LPA levels in ATX heterozygous mice (8 to 12 weeks of age) with those in wt littermates. As shown in Fig. 5A and B, when the gene dosage of ATX is reduced by half, a 50% reduction in ATX activity and LPA levels is observed. The average plasma LPA level in wt animals was 181 ± 17 nM ($n = 4$), in keeping with previous results (38), versus 86 ± 14 nM ($n = 4$) in their heterozygous littermates (Fig. 5A). Plasma S1P levels in heterozygote and wt mice were not significantly different (about 250 nM; Fig. 5C), consistent with the notion that ATX has no major role in generating S1P. Collectively, these findings strongly suggest that ATX is the major LPA-producing enzyme in vivo and show that there is no physiological compensation for reduced ATX gene expression in the heterozygous animals.

DISCUSSION

Our results show that ATX is indispensable for embryonic development, as ATX-deficient embryos die at E9.5 with severely impaired vessel formation in yolk sac and embryo proper as well as other abnormalities (Table 2). Since ATX functions as a lysoPLD, our results suggest that loss of LPA production and downstream GPCR signaling is responsible for the observed phenotype. While we find that all known LPA receptors are expressed during E6.5 to E10.5 (Fig. 4B), the phenotype of individual LPA receptor knockouts (LPA_{1-3}) has not so far been associated with embryonic vascular defects (20, 56). However, an LPA-associated vascular phenotype may only become evident from triple or quadruple receptor knockouts. An alternative or additional possibility is that LPA acts on as-yet-unidentified GPCRs to influence vascular development.

In contrast, a critical role for S1P signaling in vascular development has been well established, but S1P clearly acts at later embryonic stages than ATX. S1P is essential for the stabilization of nascent vessels by smooth muscle cells at around E12.5 rather than for vessel formation per se (27, 29). Although ATX can generate S1P from SPC in vitro (7), a physiological role for ATX in sphingolipid metabolism seems unlikely, as outlined in the introduction and supported by our finding that plasma S1P levels, unlike LPA levels, are normal in ATX heterozygous animals (Fig. 5). While it remains formally possible that ATX has an additional role in extracellular nucleotide metabolism or even a role unrelated to its catalytic activity (10), our findings are most consistent with the notion that ATX-mediated LPA production in the microenvironment of endothelial cells and subsequent GPCR signaling is essential for vascular development. Consistent with this, LPA stimulates vessel formation in a GPCR-dependent manner in the chicken embryo CAM assay (C. Rivera-Lopez and K. Lynch, personal communication); furthermore, LPA promotes vascular network formation in murine E8.5 allantois explants, albeit less efficaciously than S1P (1).

How might LPA signaling govern vascular development? Impaired vascular development causing embryonic death around E9.5 has been observed in several other mutant mice, including those lacking genes involved in receptor tyrosine kinase signaling, G protein signaling, cell adhesion, migration, and oxygen sensing (for a review, see references 2 and 9), so comparison to other knockouts may provide a clue. Considering that LPA is a potent upstream activator of $G\alpha_{13}$ (and presumably $G\alpha_{12}$) (24, 30), the most relevant phenotype in this context is that of $G\alpha_{13}$ knockout and $G\alpha_{12}/G\alpha_{13}$ double-knockout mice (16, 34). As seen with ATX-deficient mice, the $G\alpha_{13}$ knockouts die around E9.5 due to impaired blood vessel formation in both yolk sac and embryo, with enlarged vessels in the head region (34). This phenotype is rescued by endothelium-specific reexpression of $G\alpha_{13}$ (37), demonstrating that $G\alpha_{13}$ signaling in endothelial cells is essential for vascular development. Combined deficiencies of $G\alpha_{13}$ and $G\alpha_{12}$ yield a somewhat earlier and more severe phenotype that includes headfold malformation, a short allantois, and unclosed and sometimes kinked neural tubes (16). $G\alpha_{13}$, probably in cooperation with $G\alpha_{12}$, links GPCRs to guanine nucleotide exchange factors for RhoA, a key regulator of the actin cytoskeleton (40), and to other effectors (36). Through its ability to regulate cell shape and adhesion, RhoA activity is fundamental to cell migration. Indeed, cells deficient in either $G\alpha_{13}$ or RhoA activity fail to migrate towards LPA (16, 50), underscoring the importance of the LPA-$G\alpha_{13}$-RhoA pathway for cell motility. LPA has multiple effects on endothelial cells, including stimulation of cell

migration and invasion (35, 53), which are critical events during angiogenesis, and an increase in endothelial monolayer permeability (33, 41). LPA also exerts migratory and contractile effects on vascular smooth muscle cells (30). Thus, ATX-mediated LPA production and subsequent LPA signaling through $G\alpha_{13}$, in cooperation with $G\alpha_{12}$ and other G proteins, may contribute to vascular development by stimulating endothelial cell migration and invasion as well as by regulating adhesive interactions with the extracellular matrix and smooth muscle cells. Consistent with this, the vascular defects observed in ATX- and $G\alpha_{13}$-deficient mice resemble those in mice lacking genes involved in cell migration and adhesion such as fibronectin and focal adhesion kinase (13, 19). Further insight into the mechanistic basis of the ATX-deficient phenotype awaits the generation and analysis of endothelium- and/or smooth muscle-specific ATX and LPA receptor knockout mice as well as transgenic rescue studies. Tissue-specific ATX knockouts will also allow assessment of how the present findings in the embryo extrapolate to the adult, where ATX and the LPA/LPA receptor axis have been implicated in several disorders, including cancer (28).

In the meantime, an interesting finding of the present study is that ATX heterozygous mice possess half as much plasma LPA as their normal littermates, consistent with ATX being the major LPA-producing enzyme in vivo and, furthermore, indicating that ATX activity is not upregulated to compensate for the *Enpp2* null allele. ATX heterozygous mice have not shown any obvious abnormalities until now and thus offer an opportunity to test several potential roles of LPA in vivo, including tumor progression, wound healing, and neurophysiological functions.

ACKNOWLEDGMENTS

We thank Junken Aoki, Richard Proia, and Kevin Lynch for sharing unpublished results; Stefan Offermanns and Mathieu Bollen for helpful discussions; and Trudi Hengeveld, Jeroen Korving, Rahmen Bin Ali, and John Zevenhoven for experimental assistance.

This work was funded by the Dutch Cancer Society (W.H.M. and J.J.) and the Wellcome Trust (M.J.O.W. and T.R.P.).

REFERENCES

1. **Argraves, K. M., B. A. Wilkerson, W. S. Argraves, P. A. Fleming, L. M. Obeid, and C. J. Drake.** 2004. Sphingosine-1-phosphate signaling promotes critical migratory events in vasculogenesis. J. Biol. Chem. **279:**50580–50590.
2. **Argraves, W. S., and C. J. Drake.** 2005. Genes critical to vasculogenesis as defined by systematic analysis of vascular defects in knockout mice. Anat. Rec. A Discov. Mol. Cell Evol. Biol. **286:**875–884.
3. **Bachner, D., M. Ahrens, N. Betat, D. Schroder, and G. Gross.** 1999. Developmental expression analysis of murine autotaxin (ATX). Mech. Dev. **84:** 121–125.
4. **Baumforth, K. R., J. R. Flavell, G. M. Reynolds, G. Davies, T. R. Pettit, W. Wei, S. Morgan, T. Stankovic, Y. Kishi, H. Arai, M. Nowakova, G. Pratt, J. Aoki, M. J. Wakelam, L. S. Young, and P. G. Murray.** 2005. Induction of autotaxin by the Epstein-Barr virus promotes the growth and survival of Hodgkin lymphoma cells. Blood **106:**2138–2146.
5. **Boucharaba, A., C. M. Serre, S. Gres, J. S. Saulnier-Blache, J. C. Bordet, J. Guglielmi, P. Clezardin, and O. Peyruchaud.** 2004. Platelet-derived lysophosphatidic acid supports the progression of osteolytic bone metastases in breast cancer. J. Clin. Investig. **114:**1714–1725.
6. **Carvalho, R. L., L. Jonker, M. J. Goumans, J. Larsson, P. Bouwman, S. Karlsson, P. T. Dijke, H. M. Arthur, and C. L. Mummery.** 2004. Defective paracrine signalling by TGFβ in yolk sac vasculature of endoglin mutant mice: a paradigm for hereditary haemorrhagic telangiectasia. Development **131:**6237–6247.
7. **Clair, T., J. Aoki, E. Koh, R. W. Bandle, S. W. Nam, M. M. Ptaszynska, G. B. Mills, E. Schiffmann, L. A. Liotta, and M. L. Stracke.** 2003. Autotaxin hydrolyzes sphingosylphosphorylcholine to produce the regulator of migration, sphingosine-1-phosphate. Cancer Res. **63:**5446–5453.
8. **Clair, T., H. Y. Lee, L. A. Liotta, and M. L. Stracke.** 1997. Autotaxin is an exoenzyme possessing 5′-nucleotide phosphodiesterase/ATP pyrophosphatase and ATPase activities. J. Biol. Chem. **272:**996–1001.
9. **Copp, A. J.** 1995. Death before birth: clues from gene knockouts and mutations. Trends Genet. **11:**87–93.
10. **Dennis, J., L. Nogaroli, and B. Fuss.** 2005. Phosphodiesterase-Iα/autotaxin (PD-Iα/ATX): a multifunctional protein involved in central nervous system development and disease. J. Neurosci. Res. **82:**737–742.
11. **Ferry, G., E. Tellier, A. Try, S. Gres, I. Naime, M. F. Simon, M. Rodriguez, J. Boucher, I. Tack, S. Gesta, P. Chomarat, M. Dieu, M. Raes, J. P. Galizzi, P. Valet, J. A. Boutin, and J. S. Saulnier-Blache.** 2003. Autotaxin is released from adipocytes, catalyzes lysophosphatidic acid synthesis, and activates preadipocyte proliferation. Up-regulated expression with adipocyte differentiation and obesity. J. Biol. Chem. **278:**18162–18169.
12. **Fuss, B., H. Baba, T. Phan, V. K. Tuohy, and W. B. Macklin.** 1997. Phosphodiesterase I, a novel adhesion molecule and/or cytokine involved in oligodendrocyte function. J. Neurosci. **17:**9095–9103.
13. **George, E. L., E. N. Georges-Labouesse, R. S. Patel-King, H. Rayburn, and R. O. Hynes.** 1993. Defects in mesoderm, neural tube and vascular development in mouse embryos lacking fibronectin. Development **119:**1079–1091.
14. **Gijsbers, R., J. Aoki, H. Arai, and M. Bollen.** 2003. The hydrolysis of lysophospholipids and nucleotides by autotaxin (NPP2) involves a single catalytic site. FEBS Lett. **538:**60–64.
15. **Goding, J. W., B. Grobben, and H. Slegers.** 2003. Physiological and pathophysiological functions of the ecto-nucleotide pyrophosphatase/phosphodiesterase family. Biochim. Biophys. Acta **1638:**1–19.
16. **Gu, J. L., S. Muller, V. Mancino, S. Offermanns, and M. I. Simon.** 2002. Interaction of G α_{12} with G α_{13} and G α_q signaling pathways. Proc. Natl. Acad. Sci. USA **99:**9352–9357.
17. **Hama, K., J. Aoki, M. Fukaya, Y. Kishi, T. Sakai, R. Suzuki, H. Ohta, T. Yamori, M. Watanabe, J. Chun, and H. Arai.** 2004. Lysophosphatidic acid and autotaxin stimulate cell motility of neoplastic and non-neoplastic cells through LPA1. J. Biol. Chem. **279:**17634–17639.
18. **Hoelzinger, D. B., L. Mariani, J. Weis, T. Woyke, T. J. Berens, W. S. McDonough, A. Sloan, S. W. Coons, and M. E. Berens.** 2005. Gene expression profile of glioblastoma multiforme invasive phenotype points to new therapeutic targets. Neoplasia **7:**7–16.
19. **Ilic, D., Y. Furuta, S. Kanazawa, N. Takeda, K. Sobue, N. Nakatsuji, S. Nomura, J. Fujimoto, M. Okada, and T. Yamamoto.** 1995. Reduced cell motility and enhanced focal adhesion contact formation in cells from FAK-deficient mice. Nature **377:**539–544.
20. **Ishii, I., N. Fukushima, X. Ye, and J. Chun.** 2004. Lysophospholipid receptors: signaling and biology. Annu. Rev. Biochem. **73:**321–354.
21. **Jansen, S., C. Stefan, J. W. Creemers, E. Waelkens, A. Van Eynde, W. Stalmans, and M. Bollen.** 2005. Proteolytic maturation and activation of autotaxin (NPP2), a secreted metastasis-enhancing lysophospholipase D. J. Cell Sci. **118:**3081–3089.
22. **Kehlen, A., N. Englert, A. Seifert, T. Klonisch, H. Dralle, J. Langner, and C. Hoang-Vu.** 2004. Expression, regulation and function of autotaxin in thyroid carcinomas. Int. J. Cancer **109:**833–838.
23. **Kingsbury, M. A., S. K. Rehen, J. J. Contos, C. M. Higgins, and J. Chun.** 2003. Non-proliferative effects of lysophosphatidic acid enhance cortical growth and folding. Nat. Neurosci. **6:**1292–1299.
24. **Kranenburg, O., M. Poland, F. P. van Horck, D. Drechsel, A. Hall, and W. H. Moolenaar.** 1999. Activation of RhoA by lysophosphatidic acid and $G\alpha_{12/13}$ subunits in neuronal cells: induction of neurite retraction. Mol. Biol. Cell **10:**1851–1857.
25. **Lee, H. Y., J. Murata, T. Clair, M. H. Polymeropoulos, R. Torres, R. E. Manrow, L. A. Liotta, and M. L. Stracke.** 1996. Cloning, chromosomal localization, and tissue expression of autotaxin from human teratocarcinoma cells. Biochem. Biophys. Res. Commun. **218:**714–719.
26. **Liliom, K., G. Sun, M. Bunemann, T. Virag, N. Nusser, D. L. Baker, D. A. Wang, M. J. Fabian, B. Brandts, K. Bender, A. Eickel, K. U. Malik, D. D. Miller, D. M. Desiderio, G. Tigyi, and L. Pott.** 2001. Sphingosylphosphocholine is a naturally occurring lipid mediator in blood plasma: a possible role in regulating cardiac function via sphingolipid receptors. Biochem. J. **355:**189–197.
27. **Liu, Y., R. Wada, T. Yamashita, Y. Mi, C. X. Deng, J. P. Hobson, H. M. Rosenfeldt, V. E. Nava, S. S. Chae, M. J. Lee, C. H. Liu, T. Hla, S. Spiegel, and R. L. Proia.** 2000. Edg-1, the G protein-coupled receptor for sphingosine-1-phosphate, is essential for vascular maturation. J. Clin. Investig. **106:**951–961.
28. **Mills, G. B., and W. H. Moolenaar.** 2003. The emerging role of lysophosphatidic acid in cancer. Nat. Rev. Cancer **3:**582–591.
29. **Mizugishi, K., T. Yamashita, A. Olivera, G. F. Miller, S. Spiegel, and R. L. Proia.** 2005. Essential role for sphingosine kinases in neural and vascular development. Mol. Cell. Biol. **25:**11113–11121.
30. **Moolenaar, W. H., L. A. van Meeteren, and B. N. Giepmans.** 2004. The ins and outs of lysophosphatidic acid signaling. Bioessays **26:**870–881.
31. **Nam, S. W., T. Clair, C. K. Campo, H. Y. Lee, L. A. Liotta, and M. L. Stracke.** 2000. Autotaxin (ATX), a potent tumor motogen, augments invasive and metastatic potential of ras-transformed cells. Oncogene **19:**241–247.

32. **Nam, S. W., T. Clair, Y. S. Kim, A. McMarlin, E. Schiffmann, L. A. Liotta, and M. L. Stracke.** 2001. Autotaxin (NPP-2), a metastasis-enhancing motogen, is an angiogenic factor. Cancer Res. **61:**6938–6944.
33. **Nieuw Amerongen, G. P., M. A. Vermeer, and V. W. van Hinsbergh.** 2000. Role of RhoA and Rho kinase in lysophosphatidic acid-induced endothelial barrier dysfunction. Arterioscler. Thromb. Vasc. Biol. **20:**E127–E133.
34. **Offermanns, S., V. Mancino, J. P. Revel, and M. I. Simon.** 1997. Vascular system defects and impaired cell chemokinesis as a result of $G\alpha_{13}$ deficiency. Science **275:**533–536.
35. **Panetti, T. S., D. F. Hannah, C. Avraamides, J. P. Gaughan, C. Marcinkiewicz, A. Huttenlocher, and D. F. Mosher.** 2004. Extracellular matrix molecules regulate endothelial cell migration stimulated by lysophosphatidic acid. J. Thromb. Haemost. **2:**1645–1656.
36. **Postma, F. R., K. Jalink, T. Hengeveld, S. Offermanns, and W. H. Moolenaar.** 2001. $G\alpha_{13}$ mediates activation of a depolarizing chloride current that accompanies RhoA activation in both neuronal and nonneuronal cells. Curr. Biol. **11:**121–124.
37. **Ruppel, K. M., D. Willison, H. Kataoka, A. Wang, Y. W. Zheng, I. Cornelissen, L. Yin, S. M. Xu, and S. R. Coughlin.** 2005. Essential role for $G\alpha_{13}$ in endothelial cells during embryonic development. Proc. Natl. Acad. Sci. USA **102:**8281–8286.
38. **Saulnier-Blache, J. S., A. Girard, M. F. Simon, M. Lafontan, and P. Valet.** 2000. A simple and highly sensitive radioenzymatic assay for lysophosphatidic acid quantification. J. Lipid Res. **41:**1947–1951.
39. **Schaft, J., R. Ashery-Padan, F. van der Hoeven, P. Gruss, and A. F. Stewart.** 2001. Efficient FLP recombination in mouse ES cells and oocytes. Genesis **31:**6–10.
40. **Schmidt, A., and A. Hall.** 2002. Guanine nucleotide exchange factors for Rho GTPases: turning on the switch. Genes Dev. **16:**1587–1609.
41. **Schulze, C., C. Smales, L. L. Rubin, and J. M. Staddon.** 1997. Lysophosphatidic acid increases tight junction permeability in cultured brain endothelial cells. J. Neurochem. **68:**991–1000.
42. **Siess, W., and G. Tigyi.** 2004. Thrombogenic and atherogenic activities of lysophosphatidic acid. J. Cell. Biochem. **92:**1086–1094.
43. **Stassar, M. J., G. Devitt, M. Brosius, L. Rinnab, J. Prang, T. Schradin, J. Simon, S. Petersen, A. Kopp-Schneider, and M. Zoller.** 2001. Identification of human renal cell carcinoma associated genes by suppression subtractive hybridization. Br. J. Cancer **85:**1372–1382.
44. **Stefan, C., S. Jansen, and M. Bollen.** 2005. NPP-type ectophosphodiesterases: unity in diversity. Trends Biochem. Sci. **30:**542–550.
45. **Stracke, M. L., H. C. Krutzsch, E. J. Unsworth, A. Arestad, V. Cioce, E. Schiffmann, and L. A. Liotta.** 1992. Identification, purification, and partial sequence analysis of autotaxin, a novel motility-stimulating protein. J. Biol. Chem. **267:**2524–2529.
46. **Su, A. I., M. P. Cooke, K. A. Ching, Y. Hakak, J. R. Walker, T. Wiltshire, A. P. Orth, R. G. Vega, L. M. Sapinoso, A. Moqrich, A. Patapoutian, G. M. Hampton, P. G. Schultz, and J. B. Hogenesch.** 2002. Large-scale analysis of the human and mouse transcriptomes. Proc. Natl. Acad. Sci. USA **99:**4465–4470.
47. **Tokumura, A., E. Majima, Y. Kariya, K. Tominaga, K. Kogure, K. Yasuda, and K. Fukuzawa.** 2002. Identification of human plasma lysophospholipase D, a lysophosphatidic acid-producing enzyme, as autotaxin, a multifunctional phosphodiesterase. J. Biol. Chem. **277:**39436–39442.
48. **Umezu-Goto, M., Y. Kishi, A. Taira, K. Hama, N. Dohmae, K. Takio, T. Yamori, G. B. Mills, K. Inoue, J. Aoki, and H. Arai.** 2002. Autotaxin has lysophospholipase D activity leading to tumor cell growth and motility by lysophosphatidic acid production. J. Cell Biol. **158:**227–233.
49. **van der Weyden, L., D. J. Adams, L. W. Harris, D. Tannahill, M. J. Arends, and A. Bradley.** 2005. Null and conditional semaphorin 3B alleles using a flexible puroDeltatk loxP/FRT vector. Genesis **41:**171–178.
50. **Van Leeuwen, F. N., C. Olivo, S. Grivell, B. N. Giepmans, J. G. Collard, and W. H. Moolenaar.** 2003. Rac activation by lysophosphatidic acid LPA1 receptors through the guanine nucleotide exchange factor Tiam1. J. Biol. Chem. **278:**400–406.
51. **van Meeteren, L. A., F. Frederiks, B. N. Giepmans, M. F. Pedrosa, S. J. Billington, B. H. Jost, D. V. Tambourgi, and W. H. Moolenaar.** 2004. Spider and bacterial sphingomyelinases D target cellular lysophosphatidic acid receptors by hydrolyzing lysophosphatidylcholine. J. Biol. Chem. **279:**10833–10836.
52. **van Meeteren, L. A., P. Ruurs, E. Christodoulou, J. W. Goding, H. Takakusa, K. Kikuchi, A. Perrakis, T. Nagano, and W. H. Moolenaar.** 2005. Inhibition of autotaxin by lysophosphatidic acid and sphingosine 1-phosphate. J. Biol. Chem. **280:**21155–21161.
53. **Wu, W. T., C. N. Chen, C. I. Lin, J. H. Chen, and H. Lee.** 2005. Lysophospholipids enhance matrix metalloproteinase-2 expression in human endothelial cells. Endocrinology **146:**3387–3400.
54. **Yancopoulos, G. D., S. Davis, N. W. Gale, J. S. Rudge, S. J. Wiegand, and J. Holash.** 2000. Vascular-specific growth factors and blood vessel formation. Nature **407:**242–248.
55. **Yang, S. Y., J. Lee, C. G. Park, S. Kim, S. Hong, H. C. Chung, S. K. Min, J. W. Han, H. W. Lee, and H. Y. Lee.** 2002. Expression of autotaxin (NPP-2) is closely linked to invasiveness of breast cancer cells. Clin. Exp. Metastasis **19:**603–608.
56. **Ye, X., K. Hama, J. J. Contos, B. Anliker, A. Inoue, M. K. Skinner, H. Suzuki, T. Amano, G. Kennedy, H. Arai, J. Aoki, and J. Chun.** 2005. LPA3-mediated lysophosphatidic acid signalling in embryo implantation and spacing. Nature **435:**104–108.